IRAQI JOURNAL OF APPLIED PHYSICS
Vol. 22, No. 4, October-December 2026, pp. 581-585

Energy Band Diagram of ZnS/Si Heterojunction Prepared by Aqueous Solution Deposition Method

Sabah S. Hamdi [1]*
Huda S. Ali [2]
Iftikhar M. Ali [3]

[1] College of Science, University of Tikrit, Tikrit, IRAQ
[2] Department of Renewable Energy, College of Energy and Environmental Sciences, Al-Karkh University of Science, Baghdad, IRAQ
[3] Department of Physics, College of Science, University of Baghdad, Al-Jadiriyah, Baghdad, IRAQ
* Corresponding author email: Sabah.S.Hamdi@tu.edu.iq

In this work, a p-n junction was created by preparing a thin layer of ZnS, an n-type semiconductor, on a p-type silicon substrate. The 200°C temperature. The ZnS thin films' polycrystalline nature of the wurtzite-hexagonal type and favored growth direction (100) were revealed by the X-ray diffraction. The direct optical energy gap of 3.64 eV for ZnS thin films was demonstrated using optical properties. The cross-sectional measurement of the ZnS film revealed that its thickness was 322.45 nm. Voltage-current characteristics show the behavior of the diodes and the built-in voltage was also ascertained by capacitance-voltage measurements. The constructed heterojunction's band diagram (np) is assumed in this investigation.

Keywords: Zinc sulfide; Substrate temperature; Activation energy; Band diagram

1. Introduction

The Greek term "sphalerite," which suggests that it has no common resemblance to other minerals, describes zinc sulfide (ZnS), a mineral sulfide compound. Its yellow, clear, or semi-transparent chemical formula is ZnS [1]. In addition to being low toxicity, when its sublimation is low, it does not dissolve and dissolves in acids but not in water. With appropriate grafting, ZnS may be created in the almost visible range, making it an ideal illuminating material with a broad energy gap [2]. Two types of ZnS are distinguished by their composition: The most stable phase at room temperature is the cubic phase (zincblende) and the hexagonal phase (wurtzite) can be reached by heating it to 1293K at pressure of air. The hexagonal phase, also known as wurtzite, is the most preferred form of ZnS due to its superior visual characteristics and ability to function as a sulfide. ZnS is utilized in lasers, the industry for diodes that generate blue light, as well as coatings that are anti-corrosive and anti-reflective. Additionally, television and X-ray displays may be made using it [3].

2. Experimental Part

In order to prepare solutions for the production of zinc sulfide (ZnS) films, aqueous zinc nitrate ($Zn(NO_3)_2.6H_2O$) is a powder material with a molecular weight of 297.384 g/mol, a white powder of rapidly water soluble masses, a purity of 99.9%, and thiourea ($SC(NH_2)_2$), a material that is 98% pure and has a molecular weight of 76.614 g/mol. In order to create the first solution, 1.486 g of zinc nitrate were dissolved in 100 ml of distilled water at room temperature at a concentration of 0.05 M. 0.1 M was the concentration at which the second solution was prepared. 0.076 g of thiourea was dissolved in 100 ml of distilled water to create the second solution, which was at room temperature and had a concentration of 0.01 M. After mixing the solutions, a magnetic stirrer was employed to make sure the solutions were completely dissolved. The solutions are left on the magnetic mixer for ten minutes until they are uniform and plankton-free. The two solutions are then combined in an identical volumetric ratio (1:1). To guarantee full dissolve and produce a homogenous solution, the mixture is left on the magnetic mixer for an additional ten minutes.

Because it is cost-effective due to the low cost of the manufactured devices used in the preparation of these membranes and appropriate for the preparation of oxides and sulfate materials, the thermal chemical spraying method has been used to create thin films, which can be achieved by combining two or more materials with different melting points. Under typical circumstances, the thin films are made. At a temperature of 200 °C. The ZnS solution is applied to p-Si and glass substrates. Substrates and the spray device (nozzle) should be 28 cm apart since any closer and the material will evaporate before it reaches the substrate.

The thin films were deposited on substrates of p-type silicon with electrical resistivity (1-10 Ω.cm), orientation of (111), and thickness of 500 nm. These were then cut into pieces measuring 1.25x1.25 cm^2, cleaned with HF acid diluted with methanol in a ratio of (1:9), and left the slices with Si substrate in this acidic solution for a minute. The samples were then rinsed with distilled water three times to ensure that the solution remnants were disposed of, and finally dried thoroughly using cloths meant for cleaning lenses, The samples were annealed at 300 °C. After ZnS thin films were deposited at a substrate temperature of 200 °C, A FE-SEM device was used for 30 minutes to measure the cross-sectional thickness of the films. Aluminum electrodes were formed using a thermal evaporation method at low pressure ($5x10^{-5}$ mbar) and thickness of 200±20 nm, and the structure of the films was analyzed by X-ray diffraction. All prepared films were optically measured using a Shimadzu 1800 UV-Visible spectrophotometer in the wavelength range of 180–1100 nm, a 2450 Keithley electrometer for the investigation of current-voltage (I-V) characteristics, and an LCR meter (HP-R2CC4274) for the measurements of capacitance-voltage (C–V) characteristics.

3. Results and Discussion

A hexagonal system in the favored growth direction (100) was shown by the XRD findings for ZnS film at a different substrate temperature of 200 °C annealed at 300 °C for 30 minutes. The thin film X-ray diffraction patterns are displayed in Fig. (1). At angles 2θ = 26.02°, 48.167°, and 58.168°, the peak locations are (100), (110), and (201), correspondingly [4,5]. When the peak positions are compared to the zinc sulfide standard card (ICDD) 00-036-1450, table (1) displays the structural characteristics for standard peaks. According to the result, when the full-width at half maximum (FWHM) increases, the average crystallite size falls.

A decrease in the FWHM of the most-intensitve peak and an increase in the intensity of the ZnS peaks are also seen. Using the Scherer's equation (1) [7], the average crystallite size was determined, and it was between 28.42 and 44.58 nm.

$$D_{ave} = 0.9\lambda/\beta cos\theta \qquad (1)$$

The Bragg's diffraction angle is represented by θ, the FWHM (in radians) by β, and the X-ray wavelength (Kα-line) by λ = 1.5406 Å

Table (1) Structural parameters of ZnS thin film

$(2\theta)_{ICDD}$ (deg)	$(2\theta)_{exp.}$ (deg)	FWHM (rad)	(hkl)
26.915	26.023	0.22805	(100)
47.562	48.167	0.22843	(110)
57.583	58.168	0.22884	(201)

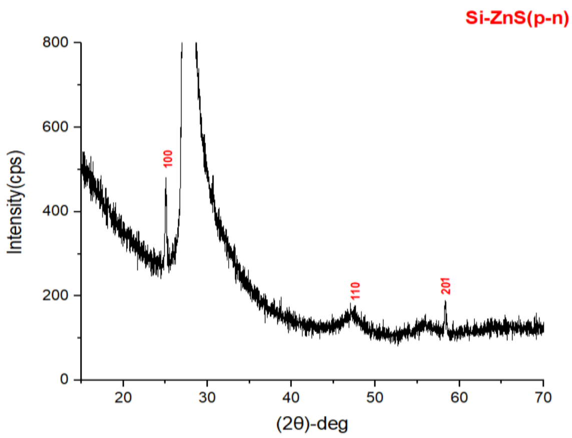

Fig. (1) XRD pattern of prepared ZnS thin film

By examining the surface morphology of the prepared thin films using field-emission scanning electron microscopy (FE-SEM), figure (2) demonstrates that the thin film structure is composed of highly ordered nanostructures with a cauliflower-like morphology, indicating controlled nucleation and uniform growth [4-6]. It was determined that the film's thickness is 322.45 nm, as illustrated in Fig. (3), and that the film's characteristics are uniform and considerably deposited using the cross-section technique in the scanning electron microscope apparatus.

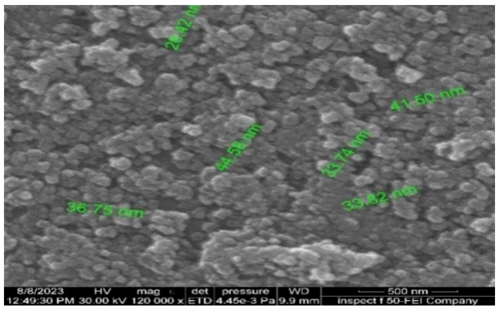

Fig. (2) FE-SEM image of prepared ZnS thin film

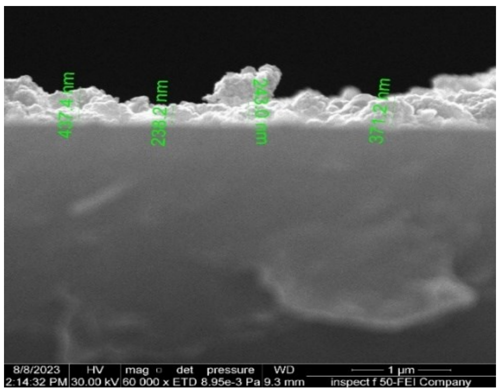

Fig. (3) Thickness of the deposited ZnS thin film

Using Eq. (2), the absorption coefficient of the prepared films was determined, and the absorption spectrum as a function of wavelength is displayed in Fig. (4a). The findings indicated that the visible region of the electromagnetic spectrum (300-700 nm) has the highest absorption; nevertheless, its energy gap is more substantial. The aforementioned remark implies that the film demonstrates elevated permeability and finds use in heterojunctions, reagents, and solar cell construction [17]. Figure (4b) shows the variation in the absorption coefficient as a function of the incident photon energy. The absorption coefficient's highest notable values are obtained at high photon energies (4-4.3 eV), indicating that electronic transitions between the valence and conduction bands may take place and that the absorption process takes place in this range, including the edge of optical absorption. The findings showed that when the produced films' photon energy increased, so did the absorption coefficient.

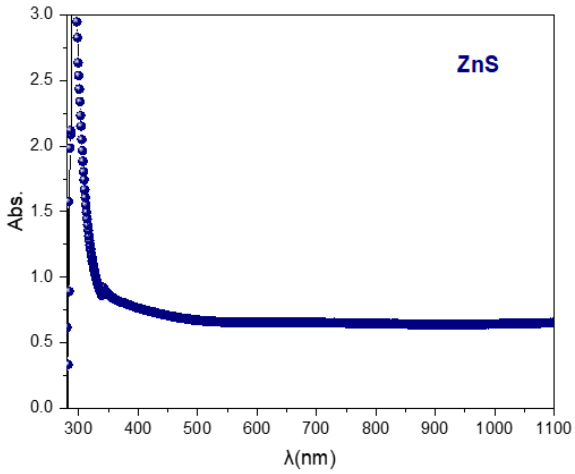

(a)

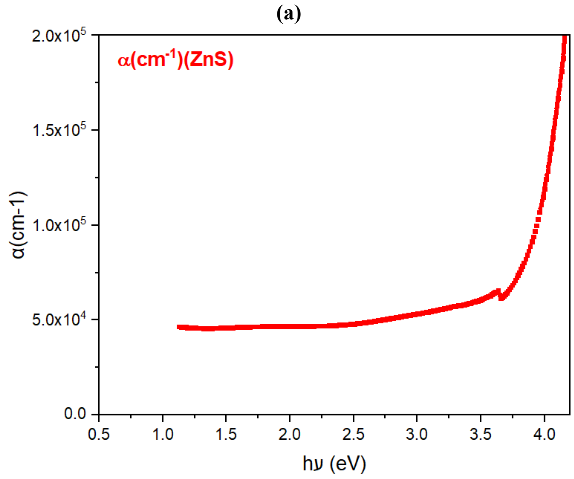

(b)

Fig. (4) (a) The absorption spectrum, and (b) the variation of absorption coefficient with incident photon energy for the prepared ZnS thin film

This aligns with the findings of other investigations [13,14]. Estimating the difference between the valence and conduction bands — which may be used to ascertain the electrical, thermal, and electronic characteristics of materials — was done by calculating the energy gap value. Equation (2) uses the Tauc formula to do the direct energy gap calculation. [11]. Taking into account that The permitted transitions are of the direct kind, meaning that the constant value (r = 1/2), and by showing how ($(\alpha h\nu)^2$) and the incident photon energy are related, as well as by extending The magnitude of the optical energy gap is shown by the straight portion of the curve that intersects the photon energy axis at ($(\alpha h\nu)^2$) = 0, as seen in Fig. (5). It was found that the optical energy gap value for the zinc sulfide (ZnS) films with a thickness of 322.45 nm was 3.64 eV, which is consistent with [12,13]

$$\alpha h\nu = \beta\left(h\nu - E_g\right)^r \qquad (2)$$

In this case, β stands for a constant, α for the absorption coefficient, hν for incident photon energy, E_g for the optical bandgap, and r=1/2 for the allowed direct transition

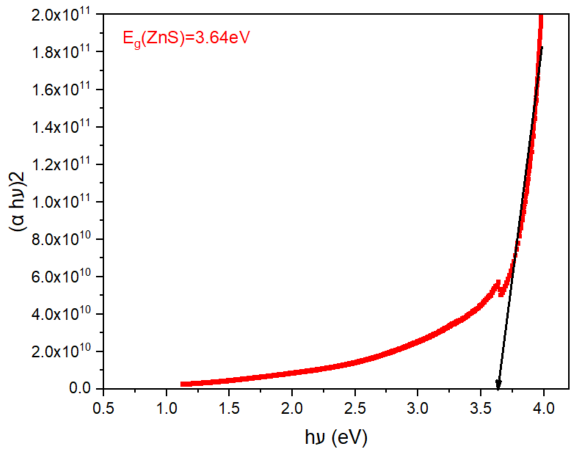

Fig. (5) Tauc's plot of the prepared ZnS thin film

The relationship between reciprocal temperature and conductivity is seen in Fig. (6). The conductivity rises with temperature between 313 and 453 K, indicating that the films are semiconductors.

The activation energy decreases as the temperature rises and hence the conductivity rises. This may be attributed to the large particle sizes and good crystallization. Generally, the crystallinity and carrier charge mobility of films are significantly affected by grain boundary scattering. The charge carrier transport mechanism in thin case caused the grain expansion to lower the grain boundary scattering [18]. This electrical conductivity may be found by using the relationship that follows:

$$\sigma_{dc} = \sigma_0 exp\left(-\frac{E_a}{k_B T}\right) \qquad (3)$$

The activation energy for conduction is represented by E_a, the temperature-independent constant by L, the Boltzmann's constant by k_B, and the absolute temperature by T. In table (2), the conductivity and activation energy values are displayed. The activation energy (E_a) is calculated using the linear relationship between Ln(σ) and 1000/T, is seen in Fig (6). Due to the presence of two interconnected areas in the ZnS thin film, the conduction mechanism is altered. Low temperatures (313–413K) are found in the first zone, whereas higher temperatures (313–453K) are found in the second [19].

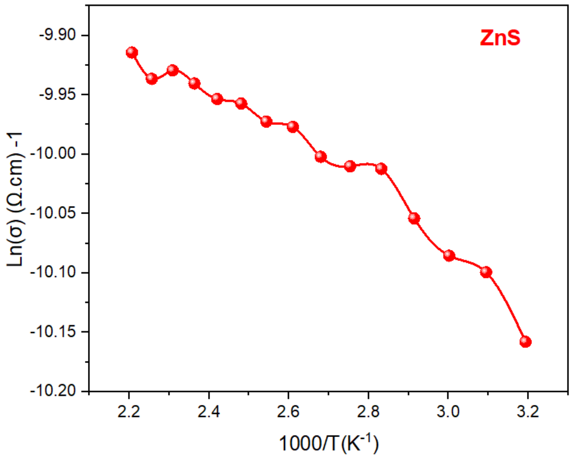

Fig. (6) Variation of Ln(σ) with 1000/T for ZnS thin film

Table (2) The activation energy and optical energy gap of the n-ZnS/p-Si structure

Sample	E_{a1}	E_{a2}	ΔE_c	ΔE_v	E_{g_1}	E_{g_2}	$V_{bi}(eV)$
np	0.3722	0.7843	0.56	1.96	1.12	3.64	0.3

Variation in capacitance has been investigated for the n-ZnS/p-Si heterojunction at a frequency of 10 kHz as a function of the forward and reverse bias voltages in the range from -1V to 1V. The junction was abrupt, as shown by the straight-line relationship between the voltage and the reciprocal squared capacitance ($1/C^2$), which is displayed in Fig. (6). Figure (7) shows that the value of built-in potential (V_{bi}) can be determined from the C-V measurement as the intersection of a straight line with the voltage axis.

The optical energy gap and DC measurement are used to create the energy beam diagram for the n-ZnS/p-Si heterojunction, as seen in Fig. (8). The n-type and p-type semiconductors will diffuse the holes from n-ZnS to p-Si at an asymmetric heterojunction (a junction) in the absence of an external voltage. While the band bends upward in p-Si due to a reduction in valence band energy, the band bends downward in ZnS because the positive ions will continue to be diffused in ZnS close to the junction [14]. Using Anderson's model, the conduction band change equals the valence band change, which is equal to ΔE_V, as seen in Fig. (8).

Plotting the energy band diagram requires the following parameters, which can be determined using equations (1) and (2) [12]:

$$\Delta E_c = \chi_1 - \chi_2 \quad (4a)$$

$$\Delta E_v = (\chi_2 + E_{g2}) - (\chi_1 + E_{g1}) = \Delta E_g - \Delta\chi \quad (4b)$$

For p-Si, the optical energy gaps is E_{g1}, and for n-ZnS, it is E_{g2} [14]. The two semiconductors are determined to have distinct energy gaps (E_g) and electron affinity values for p-Si and n-ZnS, respectively, based on experimental observations. The differences between the n- and p-type valence bands, conductivity bands, and optical energy gaps are displayed in table (2).

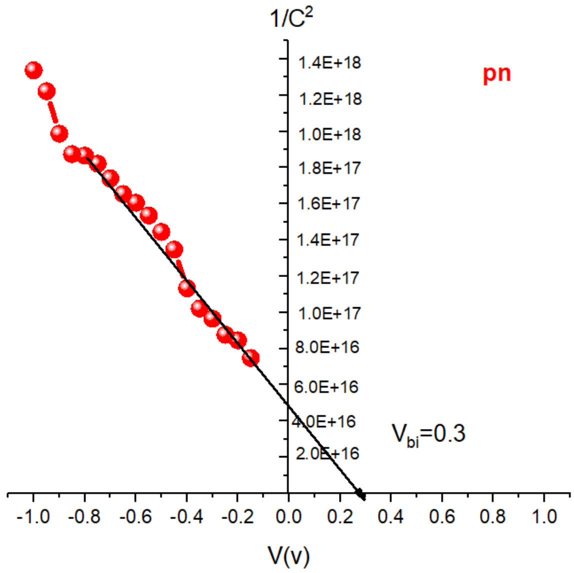

Fig. (7) Determination of built-in voltage of the n-ZnS/p-Si heterostructure

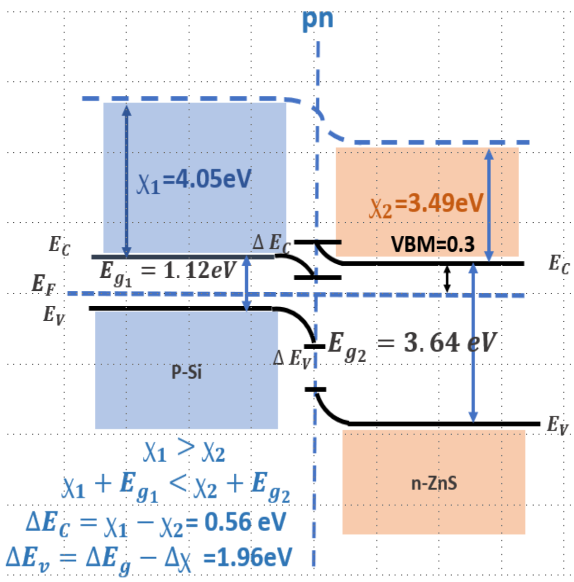

Fig. (8) Suggested band diagram of n-ZnS/p-Si heterojunction

4. Conclusion

An n-ZnS/p-Si heterojunction was successfully fabricated by depositing a polycrystalline ZnS thin film with wurtzite-hexagonal structure and preferred

(100) orientation onto a p-type silicon substrate at 200°C. The film exhibited a direct optical band gap of 3.64 eV and a thickness of 322.45 nm. Electrical measurements confirmed diode-like behavior and enabled determination of the built-in potential. These results demonstrate the potential of ZnS thin films for optoelectronic applications, particularly in UV detection and photovoltaic devices

References

[1] N. Imam and M.B. Mohamed, “Optical properties of diluted magnetic semiconductor Cu:ZnS quantum dots”, *Superlatt. Microstruct.*, 73 (2014) 203-213.

[2] W.K. Bae et al., “Highly efficient green-light-emitting diodes based on CdSe@ZnS quantum dots with a chemical-composition gradient”, *Adv. Mater.*, 21(17) (2009) 1690-1694.

[3] S.M. Sze, **"Semiconductor Devices Physics and Technology"**, (in Arabic), translated by F.G. Hayaty and H.A. Ahmed, University of Mosul, Iraq (1990).

[4] W. Daranfed et al., “Substrate Temperature Influence on ZnS Thin Films Prepared by Ultrasonic Spray”, *Thin Solid Films*, 518 (2009) 1082-1084.

[5] L.Q. Li et al., “Effect of [Zn]/[S] ratios on the Properties of Chemical Bath Deposited Zinc Sulfide Thin films”, *Appl. Surf. Sci.*, 257 (2010) 122-126.

[6] A. Ates et al., “Annealing and Light Effect on Optical and Electrical Properties of ZnS Thin Films grown with the SILAR Method”, *Mater. Sci. Semicond. Procoess.*, 10 (2007) 281-286.

[7] M. Caglar, S. Ilcan and Y. Caglar, “Influence of Substrate Temperature on Structural and Electrical Properties of ZnO Films”, *J. Sci*., 7(2) (2006) 153-159.

[8] R. Sahraei, G.M. Aval and A. Goudarzi, “Compositional, Structural and Optical Study of Nanocrystalline ZnS Thin Films Prepared by Anew Chemical Bath Deposition Route”, *Alloys Comp*., 466 (2008) 488-492.

[9] N.P. Huse et al., “An Experimental and Theoretical Study on Soft Chemically Grown CuS Thin Films for Photosensor Application”, *Mater. Sci. Semicond. Proc*ess., 67 (2017) 62-68.

[10] K. Priya et al., “A Comparative Study of Structural, Optical and Electrical Properties of ZnS Thin Films Obtained by Thermal Evaporation and SILAR Techniques”, *Ceram. Int*., 43(13) (2017) 10487-10493.

[11] M. Lopez et al., “Growth of ZnS thin films obtained by chemical spray pyrolysis: The influence of precursors”, *J. Cryst. Growth*, 285(1) (2005) 66-75.

[12] S. Mondal, S. Bhattacharyya and P. Mitra, “Effect of Al doping on the microstructure and optical band gap of ZnO thin film synthesized by successive ion layer adsorption and reaction”, *Pramana Indian J. Phys.*, 80(2) (2013) 315-326.

[13] C. Niedik et al., “Investigation on the electrical characterization of silicone rubber using D.C. conductivity measurement”, in *2016 IEEE International Conference on Dielectrics (ICD),* 2 (2016) 1114-1118.

[14] D.S. McLachlan and G. Sauti, “The A.C. and DC conductivity of nanocomposites”, *J. Nanomater.,* 2007(1) (2007), doi: 10.1155/2007/30389.

[15] S.A. Garde, “LPG and NH_3 Sensing Properties of SnO2Thick Film Resistors Prepared by Screen Printing Technique”, *Sens. Transduc. J.*, 122(11) (2010) 128-142.

[16] P.-C. Tsai, I. Pai and H. Shieh, “Two-stage chemical bath deposition for well-covered and stoichiometric ZnS thin films”, *Photovoltaic Specialists Conference (PVSC)*, 03-08 June 2012, Austin, USA, doi: 10.1109/PVSC.2012.6317987.

